Journal of Biomolecular Structure and Dynamics

ISSN: 0739-1102 (Print) 1538-0254 (Online) Journal homepage: https://www.tandfonline.com/loi/tbsd20

Synthesis, characterization, and anticancer activity of Schiff bases

Noor Uddin, Faisal Rashid, Saqib Ali, Syed Ahmed Tirmizi, Iqbal Ahmad, Sumera Zaib, Muhammad Zubair, Paula L. Diaconescu, Muhammad Nawaz Tahir, Jamshed Iqbal & Ali Haider

To cite this article: Noor Uddin, Faisal Rashid, Saqib Ali, Syed Ahmed Tirmizi, Iqbal Ahmad, Sumera Zaib, Muhammad Zubair, Paula L. Diaconescu, Muhammad Nawaz Tahir, Jamshed Iqbal & Ali Haider (2020) Synthesis, characterization, and anticancer activity of Schiff bases, Journal of Biomolecular Structure and Dynamics, 38:11, 3246-3259, DOI: 10.1080/07391102.2019.1654924

To link to this article: https://doi.org/10.1080/07391102.2019.1654924

Accepted author version posted online: 14 Aug 2019.
Published online: 28 Aug 2019.

JOURNAL OF BIOMOLECULAR STRUCTURE AND DYNAMICS
2020, VOL. 38, NO. 11, 3246–3259
https://doi.org/10.1080/07391102.2019.1654924

Synthesis, characterization, and anticancer activity of Schiff bases

Noor Uddin[a], Faisal Rashid[b], Saqib Ali[a], Syed Ahmed Tirmizi[a], Iqbal Ahmad[c], Sumera Zaib[b], Muhammad Zubair[a], Paula L. Diaconescu[d], Muhammad Nawaz Tahir[e], Jamshed Iqbal[b] and Ali Haider[a]

[a]Department of Chemistry, Quaid-i-Azam University, Islamabad, Pakistan; [b]Centre for Advanced Drug Research, COMSATS University Islamabad, Abbottabad Campus, Abbottabad, Pakistan; [c]Department of Chemistry, Allama Iqbal Open University, Islamabad, Pakistan; [d]Department of Chemistry and Biochemistry, University of California, Los Angeles, Los Angeles, CA, USA; [e]Department of Physics, University of Sargodha, Sargodha, Pakistan

Communicated by Ramaswamy H. Sarma

ABSTRACT

Five Schiff bases, 2-((3-chlorophenylimino)methyl)-5-(diethylamino)phenol (L1), 2-((2,4-dichlorophenylimino)methyl)-5-(diethylamino)phenol (L2), 5-(diethylamino)-2-((3,5-dimethylphenylimino)methyl)phenol (L3), 2-((2-chloro-4-methylphenylimino)methyl)-5-(diethylamino)phenol (L4), and 5-(diethylamino)-2-((2,6-diethylphenylimino)methyl)phenol (L5) were synthesized and characterized by elemental analysis, FT-IR, ^{1}H and ^{13}C NMR spectroscopy. Three of the compounds (L1, L2, and L4) were analyzed by single crystal X-ray diffraction: L1 and L2 crystallized in orthorhombic $P2_12_12_1$ and $Pca2_1$ space group, respectively, while L4 crystallized in monoclinic $P2_1/c$ space group. Theoretical investigations were performed for all the synthesized compounds to evaluate the structural details. Drug–DNA interaction studies results from UV–Vis spectroscopy and electrochemistry complement that the compounds bind to DNA through electrostatic interactions. The cytotoxicity of the synthesized compounds was studied against cancer cell lines (HeLa and MCF-7) and a normal cell line (BHK-21) by means of an MTT assay compared to carboplatin, featuring IC_{50} values in the micromolar range. The pro-apoptotic mechanism for the active compound L5 was evaluated by fluorescence microscopy, cell cycle analysis, caspase-9 and -3 activity, reactive oxygen species production, and DNA binding studies that further strengthen the results of that L5 is a potent drug against cancer.

ARTICLE HISTORY
Received 5 July 2019
Accepted 5 August 2019

KEYWORDS
Schiff base; DFT; electrochemistry; DNA interaction studies; antitumor activity

1. Introduction

Cancer is a multistage progressive disease, in which a group of cells start replicating in an uncontrolled fashion after a major mutation occurs in the genetic makeup of normal cells(Amiri et al., 2018; Zehra, Shavez Khan, Ahmad, & Arjmand, 2019). Genes regulating cellular growth, reproduction, and cell cycle get mutated and turn normal cells into cancerous cells (Hyndman, 2016). Such cells bypass cell check points, evade from apoptosis, produce larger populations, enlarge their mass, and start invasion into nearby and accessible tissues (Kim, 2015). Cancerous disease affects almost all body systems, organs, and tissues, except dead cells like hair and nails, and is being continuously detected in individuals of all age groups. After affecting a specific body part or system, the disease progresses to other areas of the body as well. Cancer can be managed and treated effectively if diagnosed early, but it can be fatal if it remains undiagnosed and the disease progresses to an end stage (Virnig, Baxter, Habermann, Feldman, & Bradley, 2009). There are more than 270 types of cancer that have a great tendency to resist chemotherapeutics, leading to a relapse after an initial cure. Therefore, the discovery of novel molecules and strategies to combat this challenge is necessary (Cree & Charlton, 2017; Hassanpour & Dehghani, 2017). Apoptosis, a natural death process for injured, old, or abnormal cells that prevents the development of cancer, is diminished or blocked in cancerous cells, and can be triggered again by anticancer drugs. Thus, the induction of apoptosis in cancer cells is a propitious target to be achieved by a novel molecule while carrying out anticancer studies (Olsson & Zhivotovsky, 2011).

Schiff bases or azomethines are compounds formed by a condensation reaction between primary amines and aldehydes, and have various biological, medicinal, clinical, pharmacological, and analytical applications (Dehkhodaei, Sahihi, & Amiri Rudbari, 2018; Deshmukh, Soni, Kankoriya, Halve, & Dixit, 2015; Goel, Kumar, & Chandra, 2014; Jeyaraman, Alagarraj, & Natarajan, 2019; Kumaran, Priya, Gowsika, Jayachandramani, & Mahalakshmi, 2013). They are popular ligand precursors due to their versatility and ease of preparation(Rambabu, Pradeep Kumar, Ganji, Daravath, & Shivaraj, 2019; Shahraki & Heydari, 2018; Shahraki, Shiri, & Saeidifar, 2018; Shokohi-Pour, Chiniforoshan, Sabzalian, Esmaeili, & Momtazi-Borojeni, 2018). Aromatic primary amines can also contain additional donor functional groups like –Cl, –OH, $–CH_3$, etc., which help enhancing and

CONTACT Iqbal Ahmad iqbalahmadchem@gmail.com Department of Chemistry, Allama Iqbal Open University, Islamabad 44000, Pakistan; Jamshed Iqbal drjamshed@cuiatd.edu.pk Centre for Advanced Drug Research, COMSATS University Islamabad, Abbottabad Campus, Abbottabad-22060, Pakistan; Ali Haider ahaider@qau.edu.pk Department of Chemistry, Quaid-i-Azam University, Islamabad 45320, Pakistan.

regulating biological activities (Alaghaz & Bayoumi, 2013; Siddiqui, Iqbal, Ahmad, & Weaver, 2006). Schiff bases have been shown to exhibit anticancer, antimycobacterial, antibacterial, antidepressant, and analgesic properties (Kajal, Bala, Kamboj, Sharma, & Saini, 2013).

In the present study, azomethines were synthesized and explored for their antineoplastic effect on HeLa and MCF-7 cancer cell lines, while cytotoxicity to normal cells was evaluated on BHK-21 cell line by using an MTT viability assay. The pro-apoptotic mechanism for active compounds were evaluated by fluorescence microscopy, cell cycle analysis, caspase-9 and -3 activity, reactive oxygen species production, and DNA binding studies.

2. Experimental

2.1. Materials and instrumentation

Reagents, 4-(*N*-diethylamino)salicylaldehyde (98%), 3-chloroaniline (99%), 2,4-dichloroaniline (99%), 2,3-dimethylaniline (99%), 2-chloro-4-methylaniline (98%) and 2,6-diethylaniline (98%) were purchased from Sigma Aldrich (USA) and were used without additional purification. Reagent grade solvents were dried according to a literature procedure (Armarego, 2017). A Gallenkamp (UK) electrothermal melting point apparatus was used for the determination of melting points. CHN analysis was done using a CE-440 Elemental Analyzer (Exeter Analytical, Inc.). FT-IR spectra were recorded on a Bruker Tensor II instrument. ^{1}H and ^{13}C NMR spectra were obtained by using a Bruker-300 MHz FT-NMR spectrometer with DMSO-d6 as a solvent [^{1}H (DMSO) = 2.50 ppm and ^{13}C (DMSO) = 40 ppm] (Gottlieb, Kotlyar, & Nudelman, 1997). Crystal analysis was done by using a Bruker Smart Apex II CCD-Single X-ray diffractometer (Mo X-ray source).

2.2.1. Synthesis of Schiff bases

Schiff bases were synthesized by the condensation reaction of 4-(diethylamino)-2-hydroxy benzaldehyde with R-amines (R-amine = 3-chlorobenzenamine, 2,4-dichlorobenzenamine, 3,5-dimethylbenzenamine, 2-chloro-4-mehtylbenzenamine, and 2,6-diethylbenzenamine, 20 mM each) in dried ethanol at reflux conditions and stirred for 6–7 h (Scheme 1). The precipitates obtained were filtered on Whatman filter paper and washed several times with ethanol, diethyl ether, and dried in a vacuum desiccator.

2.2. Computational details

The computational calculations were accomplished by using the DFT approach to optimize the structures in the gas phase (Alyar et al., 2019). The Gaussian 09 package was used to visualize all the theoretical results (Frisch et al., 2009). The chemical shift (δ) values were calculated from the optimized geometries by employing the Gauge Independent Atomic Orbital (GIAO) with B3LYP functional and LANL2DZ basis set (Kutzelnigg, Fleischer, & Schindler, 1990). Moreover, the fundamental vibrational frequencies were also evaluated for comparison with experimentally determined values by using the Gauss view software package.

2.3. DNA binding studies

DNA interaction ponders of the foremost strong compounds were performed following a published strategy (Iqbal, Ejaz, Saeed, & Al-Rashida, 2018; Sirajuddin, Ali, McKee, Zaib, & Iqbal, 2014). Briefly, the concentration of mammalian DNA was estimated at 260 nm using a FLUOstar Omega microplate reader (BMG Labtech, Germany). The test compound (100 μM) was interacted with different concentrations of hs-DNA (herring sperm) from 0 μM to 392 μM whereas the same concentrations of DNA were used in respective reference solutions. After an incubation of 10 min, the absorption spectra were recorded in 96 well plates with the path length of 5.5 mm.

2.4. Electrochemical studies

Electrochemical studies were performed using a Corrtest CS (Potentiostat/Galvanostat) Electrochemical Workstation, China, in a DMSO solution containing 0.1 M TBAP (tetrabutylammonium perchlorate) as a supporting electrolyte in a three-electrode cell under an argon saturated environment. A saturated silver/silver chloride was used as a reference electrode, Pt as a counter electrode and glassy carbon (GC) as a working electrode with a diameter of 0.03 cm^2. Before starting the experiment, the GC electrode was washed with

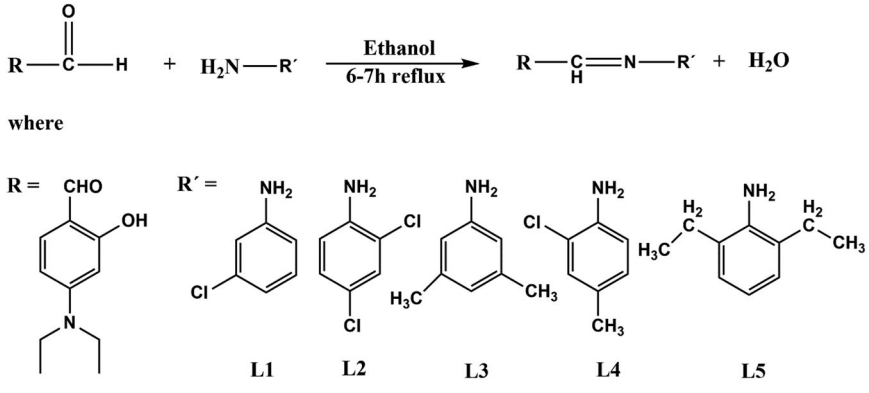

Scheme 1. General synthesis of Schiff bases (L1–L5).

an aqueous suspension of alumina (Al_2O_3) on a nylon buffing pad with deionized water at room temperature (25 °C).

2.5. Cell viability assay (MTT assay)

The cytotoxic potential of the test analogues was evaluated in the human breast adenocarcinoma cells MCF-7, human cervical adenocarcinoma cells HeLa by an MTT (dimethyl-2-thiazolyl-2,5-diphenyl-2*H*-tetrazolium bromide) based cell viability assay as described previously (Mosmann, 1983; Niks, 1990). The impact of these derivatives was moreover inspected against normal cells, i.e. child hamster kidney cells (BHK-21). Briefly, the cells (1×10^4) were cultured in a volume of 90 µL in each well of a 96-well flat-bottom culture plate and kept in a 5% CO_2 incubator at 37 °C. After an overnight incubation, the cells were treated with the test compounds (100 µM) and incubated thereafter for 24 h. The media was aspirated and 10 µL MTT (2 mg/mL) along with 90 µL media was added to each well. The plate was incubated for 4 h at 37 °C and 5% CO_2, followed by the addition of 100 µL of the reagent (1:1 solution of 50% isopropanol and 10% sodium dodecyl sulfate prepared in 0.1 N HCl). The plate was further incubated for 30 min at 37 °C and the optical density was observed at 570 nm while a background reading was done at 630 nm using a microplate reader (Bio-Tek ELx 800™, Winooski, USA). The experiment was carried out in triplicate and the results were calculated as percent inhibition values with the mean of three independent values (±SEM). The derivatives that exhibited equal to or more than 50% inhibition were further evaluated for their inhibitory concentration (IC_{50}) values.

2.6. Cell cycle analysis assay

The treated cells were subjected to a cell cycle analysis by flow cytometry, using the method as reported earlier (Saito et al., 2010). Initially, the cells (2×10^5 cells/mL) were treated with the most potent derivatives obtained from the MTT assay from the selected series and incubated overnight at 37 °C. Then, the pellets of cells were attained by centrifugation at 4000 g (for 5 min) and, after that, the pellets were resuspended in a 3% FBS solution (200 µL) that contained 5 µL of propidium iodide (20 µg/mL), 0.1% (v/v) Triton X-100, and ribonuclease A (10 µL, 10 mg/mL). The samples were analyzed by a BD Accuri flow cytometry as described earlier (Iqbal et al., 2018).

2.7. Microscopic analysis of apoptosis

The microscopic analysis of the most potent derivative was carried out to support the flow cytometry results. The analysis was done according to a previously reported method (Iqbal et al., 2018, Lin et al., 2013). The confluent cells (2×10^5 cells/well) were treated with the test compound (100 µM) and kept in a 5% CO_2 incubator at 37 °C. After 24 h, the culture medium was removed, and cells were washed thrice with cold PBS (phosphate buffered saline). Then, the cells were treated with 4% formalin and 0.1% Triton X–100. Finally, after a 5 min room incubation, 10 µL (0.1 mg/mL) of 4′,6-diamidino-2-phenylindole (DAPI) or propidium iodide (PI) dye was mixed to stain the nuclear material. The glass slides were kept in the dark for 10 min and images were captured by using a fluorescence microscope (Nikon ECLIPSE Ni–U) at an excitation/emission wavelength of 350/460 and 493/632 nm for DAPI and PI, respectively.

2.8. Determination of intracellular reactive oxygen species (ROS) production

The initiation of the production of ROS within HeLa cells of the most potent compound L5 by the different concentrations (IC_{50} value, i.e. 21 µM and 2× IC_{50}, i.e. 42 µM) was studied by using dichlorofluorescin diacetate (H2DCF-DA) dye and observed by fluorescence microscopy. Figure 12 shows that treated HeLa cells with potent compound L5 exhibit disintegrated cell membranes and condensed cellular protein (DNA) that may be due to oxidation of lipids and proteins as reported previously (Rastogi, Singh, Hader, & Sinha, 2010).

2.9. Apoptosis assessment by caspase-9 and -3 activity

Caspase-9/3 activity was analyzed using a fluorometric assay kit (Abcam). Cells were plated at 1×10^6 cells per well per 3 mL in a 6 well plate for overnight incubation. Fresh media was introduced after the removal of old media and cells were treated with the compound of interest. After 18 h, cells were collected, centrifuged, and lysed using 50 µL of lysis buffer on ice for 10 min, and incubated with DEVD-AFC substrate for caspase-3 (Lin, Lin, Hsueh, Chou, & Wong, 2018) and with LEHD-AMC substrate for caspase-9 (Pan, Xu, & Yeung, 2001) and reaction buffer at 37 °C for 3 h. The amount of fluorescent cleavage product was measured using a fluorescence microplate reader (FLUOstar Omega, BMG Labtech, Germany). All these experiments were performed in triplicate.

3. Results and discussion

The Schiff bases (L1–L5) synthesized as described above were dried and characterized by elemental analysis, FT-IR, ^1H and ^{13}C NMR spectroscopic techniques. The elemental analysis (C, H, N) results were in good agreement with those calculated for the suggested formula. The sharp melting points obtained indicate the purity of the synthesized compounds. The structures of compounds (L1–L5) along with numbering are given in Chart 1.

3.1. Infrared spectroscopy

In the IR spectra of L1–L5 show a sharp band at 3340 cm^{-1} (L1), 3386 cm^{-1} (L2), 3346 cm^{-1} (L3), 3374 cm^{-1} (L4) and 3364 cm^{-1} (L5) that is assigned to free Ar–OH. A strong band attributable to C = N is observed at 1605 cm^{-1} (L1), 1621 cm^{-1} (L2), 1600 cm^{-1} (L3), 1609 cm^{-1} (L4) and 1605 cm^{-1} (L5). The stretching vibration of medium intensity

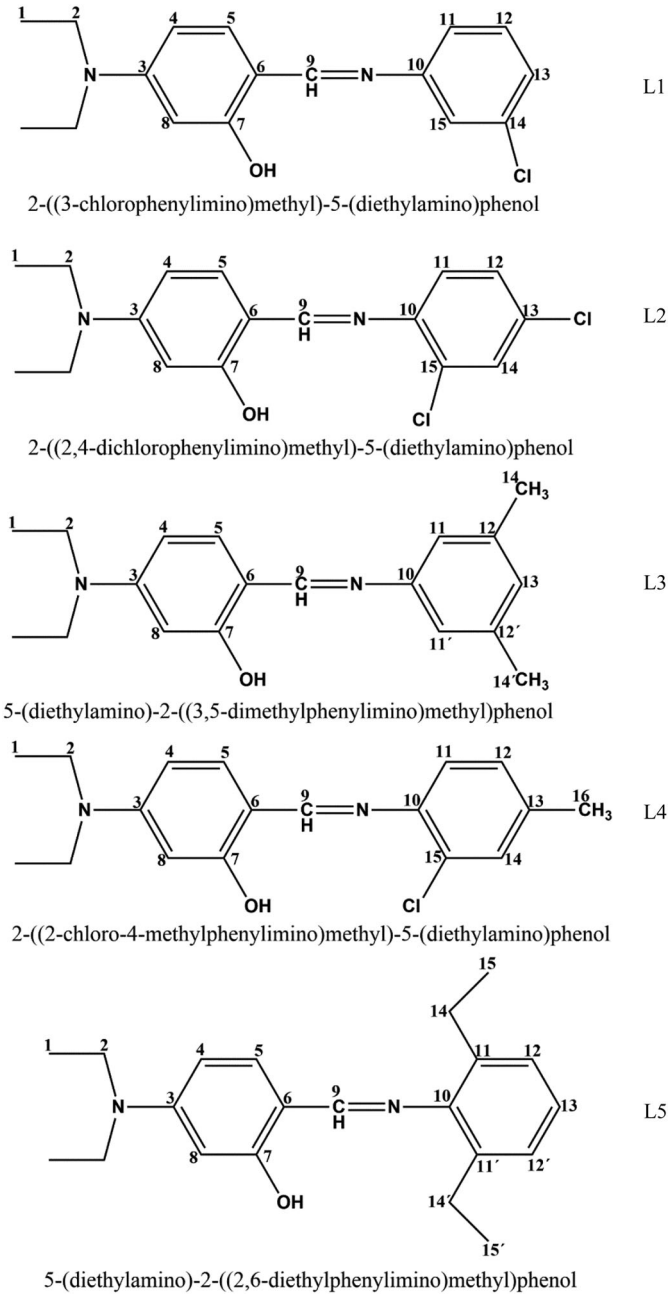

Chart 1. Structures and numbering of L1–L5.

for N–C bond occurs at 1244 cm^{-1} (L1), 1235 cm^{-1} (L2), 1240 cm^{-1} (L3), 1241 cm^{-1} (L4) and 1236 cm^{-1} (L5), while a weak intensity peak for the stretching vibration of C = C is observed at 1575 cm^{-1} (L1), 1593 cm^{-1} (L2), 1573 cm^{-1} (L3), 1581 cm^{-1} (L4) and 1584 cm^{-1} (L5).

3.2. NMR spectroscopy

The NMR spectra of compounds L1–L5 were recorded in dimethyl sulfoxide (DMSO). The chemical shifts of the different types of protons and carbons are given in the experimental part (Chart 1). The formation of L1–L5 was supported by the appearance of a sharp singlet corresponding to the azomethine proton (–N = C*H*–) at 9.64, 8.73, 8.66, 8.71, 8.25 ppm, respectively. The hydroxyl proton gives a broad singlet at 13.31, 13.50, 13.77, 13.73, 13.13 ppm, respectively. This downfield shifting of the OH proton is due to strong intramolecular O–H–N hydrogen bonding, to which the chemical shift of the proton is very sensitive (Sirajuddin, Ali, Shah, Khan, & Tahir, 2012). In the ^{13}C NMR spectra, the peak at 163.17, 162.96, 161.39, 161.79, and 163.28 ppm, respectively, belongs to the azomethine carbon (*C*H = N). The remaining peaks are described in the same positions as calculated by incremental methods (Popovic, Roje, & Pavlovic, 2001).

3.3. Crystal structures

The molecular structures of the compounds L1, L2, and L4 were authenticated by single crystal X-ray diffraction analysis. The solid-state molecular structures along with selected

distances and angles of L1, L2, and L4 are shown in Figures 1–3, respectively. Compound L1 crystalized as a monomer and L2 as a dimer in an orthorhombic crystal system having the space group $P2_12_12_1$ and $Pca2_1$, while L4 also crystalized as a dimer in a monoclinic crystal system with the space group $P2_1/c$. Unit cells and hydrogen bonding of compounds L1, L2, and L4 are shown in Figures 1–3, respectively. The phenyl ring of all the compounds having bond length ranging from 1.367 to 1.402 Å denoting aromatic character. All the compounds have one dimensional polymeric chain through intermolecular H-bonding. These compounds are stable through intramolecular hydrogen bonding between hydroxyl group and nitrogen (O1–H1 ··· N1) (Table 1).

3.4. Electronic structure studies

The L5 solution was freshly prepared just before the measurements. The absorption study of L5 was performed in a phosphate buffer (pH = 7) at 298 K. In typical experiments, 2.5 mL of an L5 solution (100 μM) was placed in the cuvette and the absorbance spectra were recorded at 258–800 nm, after the addition of the stock solutions (70 μM). In these experiments, the observed absorbance was corrected for the dilutions. Prior to recording the absorbance, the sample was incubated for 10 min. The absorption spectrum of L5 shows a maximum absorption band at 355 nm assigned to $\pi \rightarrow \pi^*$ transitions of the azomethine group.

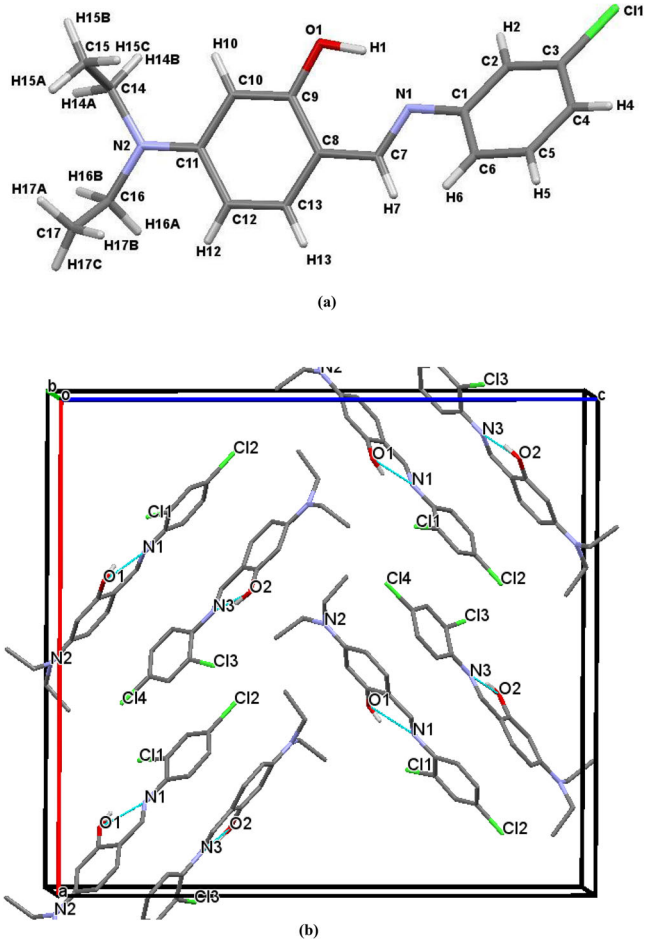

Figure 1. (a) Crystal structure of L1; (b) unit cell showing H-bonding.

3.5. Density functional theory

Quantum mechanical calculations were also carried out to support the experimental results. The computed molecular structures of the studied Schiff bases are shown in Figure 4. The distances and angles calculated from DFT studies (Table 3) are in close agreement with the experimentally determined data obtained from single crystal X-ray analysis (L1, L2, and L4).

3.5.1. Frontier molecular orbital analysis

The HOMOs (highest occupied molecular orbitals) and LUMOs (lowest unoccupied molecular orbitals) are collectively called frontier molecular orbitals and can be used to understand the course of some reactions. The frontier molecular orbitals and the energies of the HOMO and LUMO, which were computed with the B3LYP functional and using the LANL2DZ basis set of the newly synthesized Schiff bases, are depicted in Figure 5.

3.5.2. Molecular electrostatic potential

The molecular electrostatic potential (MEP) of investigated compounds (L1–L5) was predicted at the same level of theory as above to find the reactive site for electrophilic as well as nucleophilic attack. ESP analysis of the synthesized compounds (L1–L5) was done using DFT/B3LYP/6-31G(d,p). The MEP surface portrays the reactive sites in the molecules as depicted in Figure 6. The red color shows the maximum negative charge region, which indicates that an electrophilic attack is possible at this site. The site prone to nucleophilic attack is represented by the blue color indicating the maximum positive charge region, while the green color shows the zero potential region (Uddin, Siddique, Mase, Uzzaman, & Shumi, 2019). It is clear from the MEP map that the negative potential region is located over the oxygen atom (electronegative) and the positive potential region is located over the hydrogen atoms. For the oxygen atom, the negative potential represented by the deepest red color is –0.058 au (L1), –0.069 au (L2), –0.072 au (L3), –0.070 au (L4), and –0.074 au (L5), respectively, while for hydrogen atoms the positive potential represented by the deepest blue color has the same value with a positive sign.

3.6. DNA binding studies

Cancerous cells have mutated DNA and targeting it is a promising way for achieving an anti-oncogenic effect (Gurova, 2009). Small molecules can influence DNA either directly or indirectly by interacting with a protein (such as polymerases or RNA). DNA binding species can either bind covalently or non-covalently. The extent of DNA damage depends on the type of binding with DNA. Covalent binding is irreversible and most damaging. However, molecules binding through a non-covalent interaction are less toxic

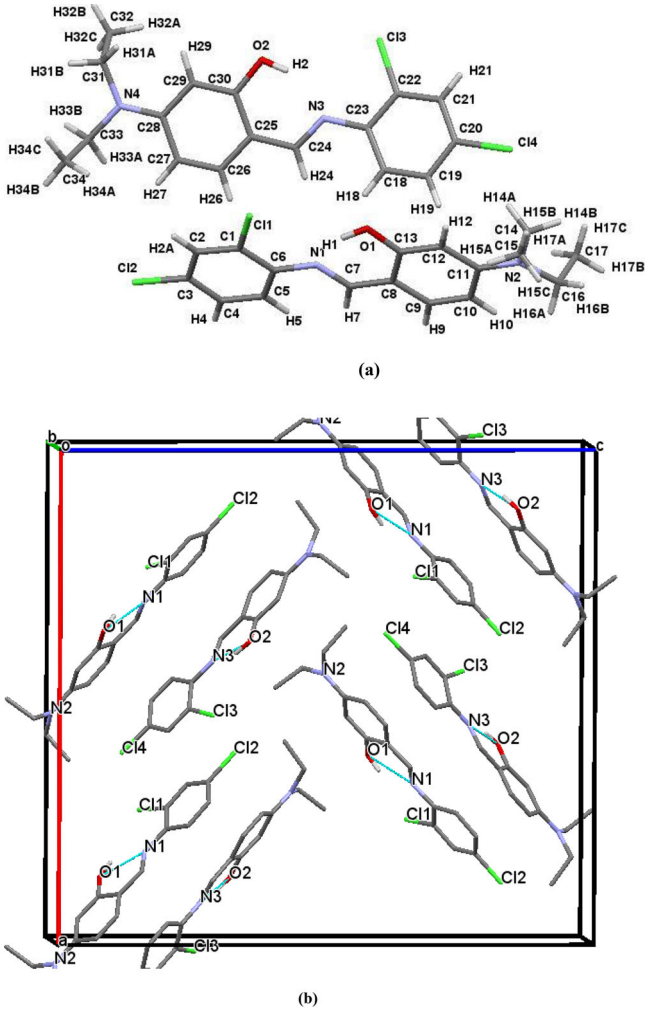

Figure 2. (a) Crystal structure of L2; (b) unit cell showing H-bonding.

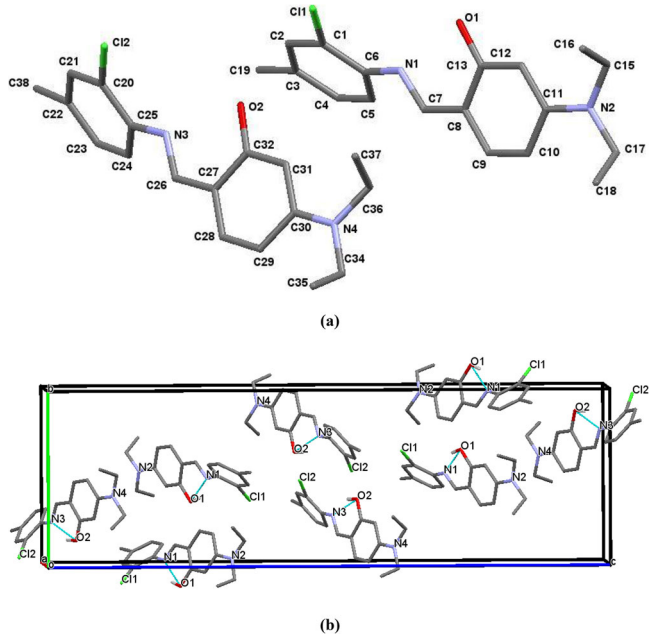

Figure 3. (a) Crystal structure of L4 (b) unit cell showing H-bonding.

(Sirajuddin, Ali, & Badshah, 2013; Zhang, Bi, Fan, Wang, & Bao, 2015). Compounds showing a DNA interaction are thus of great importance in the search of new antineoplastic molecules. The ability of L5 to interact with hs-DNA (herring sperm) was studied in the absence and presence of increasing concentrations of DNA. By increasing the DNA concentration, it is quite clear that a hyperchromicity with no red or blue shift was observed, showing a non-covalent interaction with a binding constant of $K = 2.236 \times 10^3$ M^{-1} and Gibbs free energy ΔG = –19.11 kJ/mol (Figure 7). The binding constant was calculated from the intercept to slope ratios of $A_o/A - A_o$ vs 1/[DNA] plot, while the Gibbs free energy was determined using the equation $\Delta G = -RT\ln K$.

3.7. Electrochemical studies

3.7.1. Cyclic voltammetry

The cyclic voltammetry (CV) of the compounds L1–L5 was performed using glassy carbon as a working electrode (GCE), Pt as a counter electrode and Ag/AgCl as a reference electrode, in DMSO as a solvent. Initially, the controlled CV was performed in the absence of DNA for comparison for all the Schiff bases (L1–L5) as shown in Figure 8. As clear from the CV curves, an oxidation peak for L1–L4 around 1.10 V was found. This oxidation peak is attributed to the hydroxyl moiety present in these compounds. L5 shows two oxidation peaks at 0.9 and 1.2 V along with a reduction peak at –1.2 V.

These Schiff bases were employed for further DNA binding studies as shown in Figure 9. In the presence of different concentrations of DNA, L1–L5 show a decrease in the peak currents as well as a shift in the peak potentials. The oxidation peak potential of all the compounds shifts to a more positive value. The decrease in peak current values suggests that the compounds bind to the bulky DNA molecule. The decrease in peak current and shifting of the peak potential towards a more positive potential shows the association of DNA with the Schiff bases. Due to the presence of DNA, certain changes occurred in the electrochemical response and respective current–potential parameters indicating the compound-DNA presence in the system. These changes, along with a shift toward a more positive potential, denote the electrostatic mode of interaction between the compounds and DNA (Iqbal et al., 2013; Shabbir et al., 2015).

To further evaluate the interaction between DNA and Schiff bases, CV studies were done at different scan rates. The plots of anodic peak current vs the square root of scan rate ($v^{1/2}$) for all the compounds were found linear before and after the addition of DNA with a decrease in slope for the latter case compared to the former. The diffusion of the redox species is slower in the presence of DNA and is evident from the values of the diffusion coefficient (Table 2). To support the above argument, the stability constant (K) was calculated by using the following equation (Shabbir et al., 2017):

$$1/[\mathrm{DNA}] = K(1 - \mathrm{A})/(1 - I/I_o) - K,$$

where A is an empirical constant. The K values are given in Table 2. Significantly, a large K compared to the values

Table 1. Experimental data for crystallographic analysis for compounds L1, L2 and L4.

Compound	1	2	4
Empirical formula	$C_{17}H_{19}ClN_2O$	$C_{17}H_{18}Cl_2N_2O$	$C_{18}H_{21}ClN_2O$
Formula weight	302.79	337.23	316.82
Temperature/K	296(2)	296(2)	100(2)
Crystal system	orthorhombic	orthorhombic	monoclinic
Space group	$P2_12_12_1$	$Pca2_1$	$P2_1/c$
a/Å	6.6285(4)	22.0044(19)	8.3773(4)
b/Å	15.1724(9)	6.4705(5)	10.9189(5)
c/Å	15.5972(13)	23.861(2)	34.7609(15)
α/°	90	90	90
β/°	90	90	93.342(3)
γ/°	90	90	90
Volume/Å^3	1568.61(19)	3397.3(5)	3174.2(3)
Z	4	8	8
ρ_{calc} g/cm^3	1.282	1.319	1.326
μ/mm^{-1}	0.244	0.385	2.148
F(000)	640	1408	1344
Crystal size/mm^3	0.400 × 0.340 × 0.300	0.440 × 0.300 × 0.260	0.200 × 0.080 × 0.050
Radiation	MoKα (λ = 0.71073)	MoKα (λ = 0.71073)	CuKα (λ = 1.54178)
2Θ range for data collection/°	5.37 to 55.848	3.702 to 55.906	5.092 to 139.854
Index ranges			
Reflections collected	4985	16633	25414
Independent reflections	3249 [R_{int} = 0.0380, R_{sigma} = 0.0699]	6979 [R_{int} = 0.0378, R_{sigma} = 0.0593]	5880 [R_{int} = 0.0501, R_{sigma} = 0.0409]
Data/restraints/parameters	3249/0/195	6979/1/403	5880/6/419
Goodness-of-fit on F^2	1.025	0.998	1.059
Final *R* index [I>=2σ (*I*)]	R_1 = 0.0425, wR_2 = 0.0934	R_1 = 0.0454, wR_2 = 0.1026	R_1 = 0.0399, wR_2 = 0.1000
Final *R* index [(all data])	R_1 = 0.0590, wR_2 = 0.1015	R_1 = 0.0991, wR_2 = 0.1258	R_1 = 0.0541, wR_2 = 0.1058
Largest diff. peak/hole / e Å^{-3}	0.20/–0.17	0.23/–0.23	0.34/–0.43
Flack parameter	0.11(7)	0.02(4)	

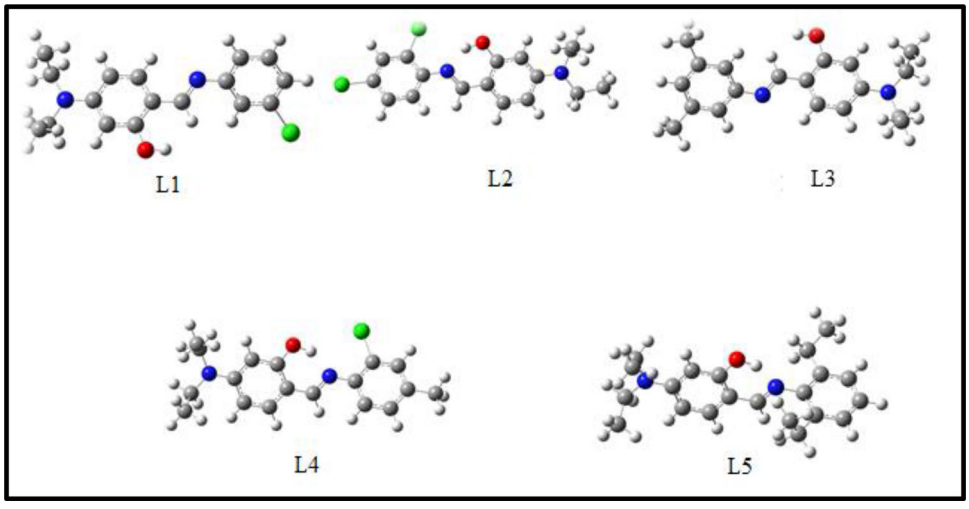

Figure 4. Optimized molecular geometries of the Schiff bases L1–L5.

Table 2. The compound-DNA interaction electrochemical parameters of compounds on glassy carbon vs. Ag/AgCl in a DMSO solution, at a 100 mVs^{-1} scan rate, at 25 °C.

Compound	D_o (cm^{2}s^{-1}) (without DNA)	D_o (cm^{2}s^{-1}) (with DNA)	K (M^{-1})	*s* (bp)
L1	5.56×10^{-6}	3.42×10^{-6}	9.76×10^{4}	2.96
L2	1.34×10^{-6}	1.90×10^{-7}	9.02×10^{4}	0.27
L3	1.90×10^{-6}	2.25×10^{-7}	4.43×10^{4}	0.73
L4	4.58×10^{-6}	2.71×10^{-6}	3.49×10^{4}	0.28
L5	5.88×10^{-5}	1.43×10^{-5}	8.37×10^{4}	1.56

Table 3. Cytotoxic efficacy of the compounds L1–L5 against HeLa, MCF-7, and BHK-21 cell lines at 100 μM.

Sample code	HeLa	MCF-7	BHK-21
	IC_{50} (μM) ± SEM/%age inhibition		
L1	2.40%	1.08%	–
L2	56.7 ± 1.45	18.0%	32.2 ± 1.78
L3	36.6%	2.57%	–
L4	4.50%	29.3%	–
L5	20.8 ± 0.46	31.0%	60.2 ± 1.33
Carboplatin	5.13 ± 0.45	89.3%	–

reported for different compounds (Arshad & Farooqi, 2018; Iqbal et al., 2013) suggests the potential ability of these Schiff base to interact with DNA. The number of binding sites (s) in terms of the concentration of base pairs is shown in Table 2 and was calculated using the following equation:

$$C_b/C_f = K[\mathrm{DNA}]/2s$$

where C_f and C_b are the concentrations of free and DNA-

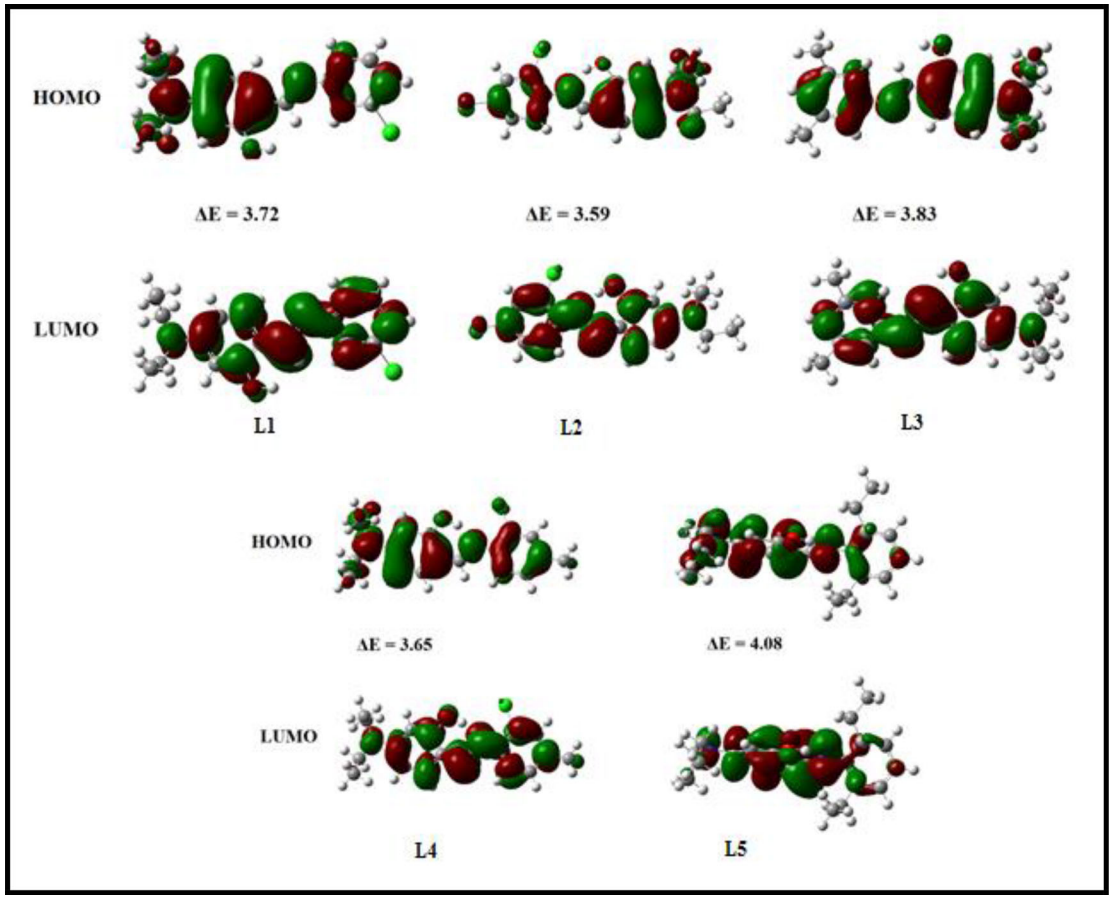

Figure 5. Frontier molecular orbitals of the Schiff bases L1–L5, along with their respective energy gap in eV.

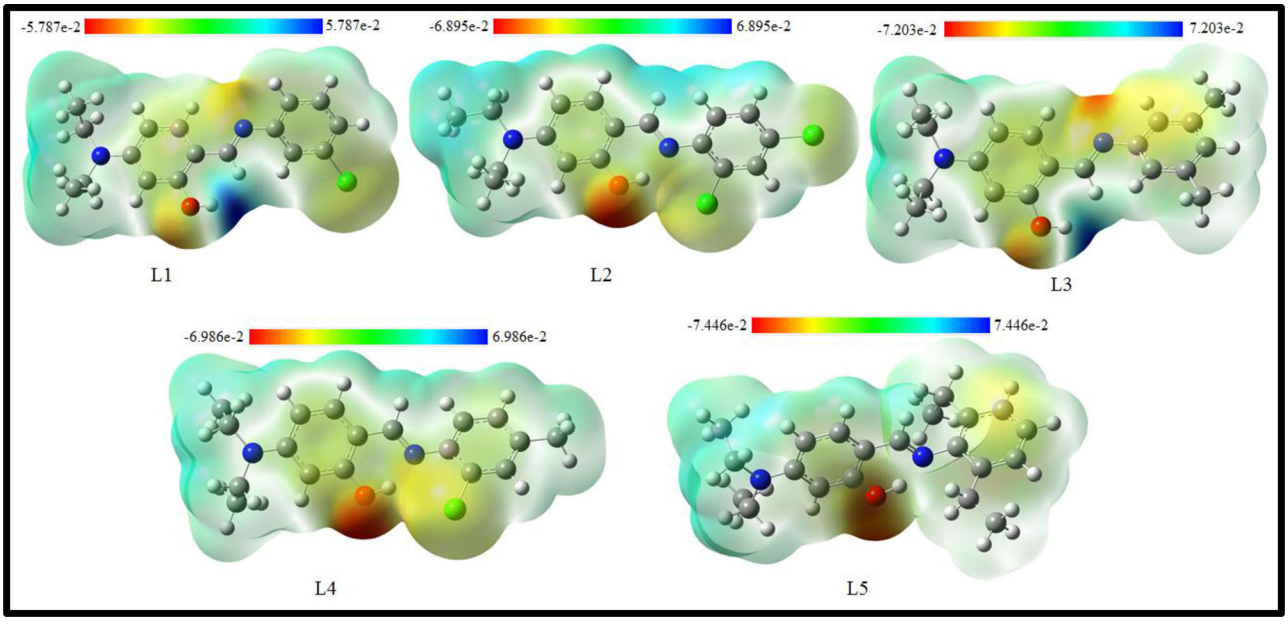

Figure 6. The molecular electrostatic potential (MEP) surfaces of the Schiff bases L1–L5.

compound bound species, respectively. Also, C_b/C_f can be represented by the equation $C_b/C_f=(I_o - I)/I$ as reported in the literature (Aslanoglu & Ayne, 2004). The values of binding site size show that L1 and L5 integrate more than one base pair of the DNA resulting in strong interactions for these compounds.

3.7.2. Differential pulse voltammetry

Differential pulse voltammograms of the Schiff bases are presented in Figure 10. Peak currents are in the order of L5 > L1 > L4 > L3 > L2 as observed by CV studies. The order is in accordance to the D_o values. The facile electron transfer (ET) process in L5 is understandable from its simple and

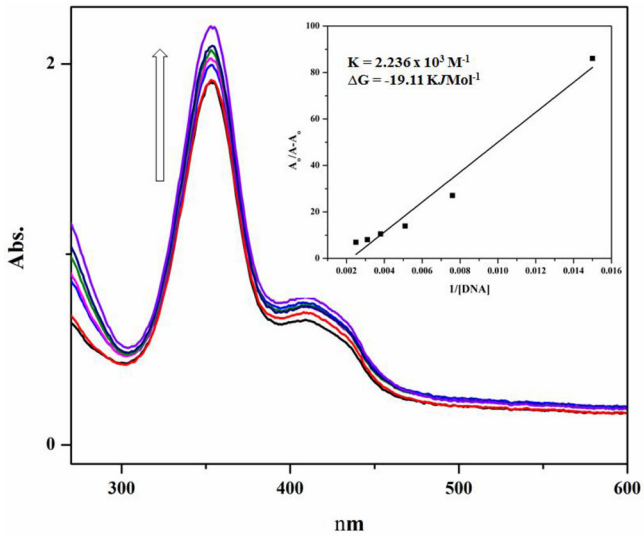

Figure 7. Absorption spectra of 100 μM of L5 in the absence (0 μM) and presence (66, 131, 196, 261, 327 and 392 μM) of DNA. The arrow direction shows increasing concentration of DNA. The graph is the plot of $A_o/(A - A_o)$ versus 1/[DNA] for the determination of the binding constant and Gibbs free energy of the L5-DNA product.

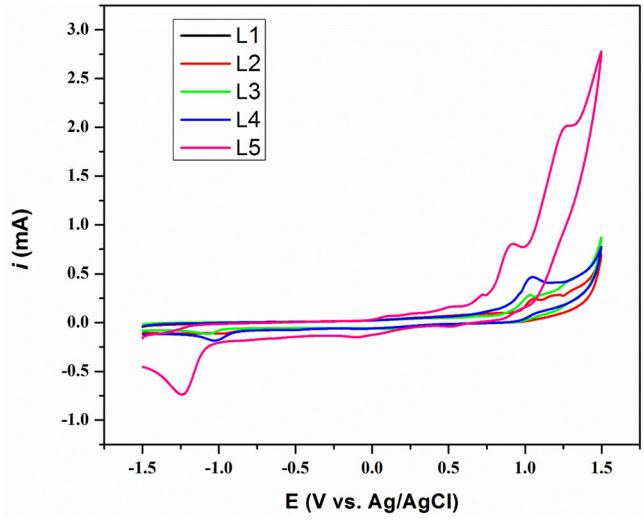

Figure 8. Cyclic voltammograms of compounds L1–L5 (1 mM each) recorded at GCE in an argon saturated DMSO + 0.1 M TBAP solution using a 100 mV s^{-1} scan rate at 25 °C.

planar structure. The observed $W_{1/2}$ values (≈200 mV) of all the five Schiff bases suggest one electron transfer process. These values are larger than the theoretical value of 90 mV for an ET process, which may be due to an uncompensated solution resistance.

3.8. Antitumor activity assay

3.8.1. Cell viability assay (MTT assay)

The cytotoxic potential of all the compounds was evaluated in human breast adenocarcinoma cells MCF-7, human cervical adenocarcinoma cells HeLa by MTT (Dimethyl-2-thiazolyl-2,5-diphenyl-2*H*-tetrazolium bromide)-based cell viability assay. Later, the effect of inhibitors showing more than 50% inhibition was also examined against normal cells, i.e. baby hamster kidney cells (BHK-21). Cells were initially treated with 100 μM end concentration, and derivatives which exhibited more than 50% inhibition were further tested in 8 dilutions to evaluate the inhibitory concentration (IC_{50} values). None of the compounds showed an inhibition equal or above 50% against the MCF-7 cell line. However, L2 and L5 exhibited more than 50% inhibition against HeLa cells, therefore, the dilution was carried out and IC_{50} values were calculated. Moreover, these compounds were tested against normal cells, i.e. baby hamster kidney cells (BHK-21) and their IC_{50} values were reported in Table 3 as well. Data is presented as the mean values (SEM) for three independent experiments. These results were revealed after a 24 h treatment of compounds with cell lines. Carboplatin used as reference control showed 5.13 ± 0.45 μM against HeLa cells, however, the compound L2 and L5 showed 56.7 ± 1.45 μM and 20.8 ± 0.46 μM, respectively.

3.8.2. Cell cycle analysis assay

Cell cycle analysis is a method to determine the DNA content in cells with a great accuracy. The assay involves the use of a fluorescent dye, propidium iodide, which enters the cells whose membranes are ruptured after treating with a cytotoxic molecule. Propidium iodide (PI) binds to genetic material such as DNA, RNA, and mitochondrial DNA. Mitochondrial DNA has a negligible amount in cytosol. To acquire only a DNA quantity in such cells, generally, RNase is added to remove RNA so that PI could not bind to it. A difference in DNA content in $G_0/1$ (gap 0 and gap1), S (synthesis), and G_2/M (gap2/checkpoint and mitosis) cell cycle phases by using this univariate analysis can help understanding the phase at which a certain molecule is causing an arrest to show its cytotoxic potential when compared to control or untreated cells (Crissman & Tobey, 1974; Darzynkiewicz, Halicka, & Zhao, 2010; Nunez, 2001). The most effective cytotoxic analogue L5 was selected for flow cytometry analysis to further investigate its effect on cell cycle progression and apoptosis in HeLa cells. Figure 11 shows the DNA content within the dividing cells as assessed by propidium iodide (PI) staining and the percent cell population within the cell cycle phases, i.e. $G_o - G_1$, S, and G_2/M phases. For this purpose, the compound was used in three different concentrations (i.e. 20, 50, and 100 μM) keeping in mind the IC_{50} values of the compound.

3.8.3. Microscopic analysis of apoptosis

Propidium iodide is a hydrophilic, light sensitive, and membrane impermeable fluorescent dye that specifically binds to nucleic acids (DNA, RNA, mitochondrial DNA) in dead or apoptotic cells, which possess a ruptured or permeable membrane, by intercalation with an almost 20 to 30-fold increase in fluorescence intensity and gives information about the integrity of cells (Crowley et al., 2016; Dengler, Schulte, Berger, Mertelsmann, & Fiebig, 1995; Sträuber & Müller, 2010). On the other hand, 4′,6-diamidino-2-phenylindole (DAPI) is a nuclear staining dye that binds to adenine-thymine rich sequences of the DNA minor groove to form a fluorescent complex while a nonfluorescent complex is

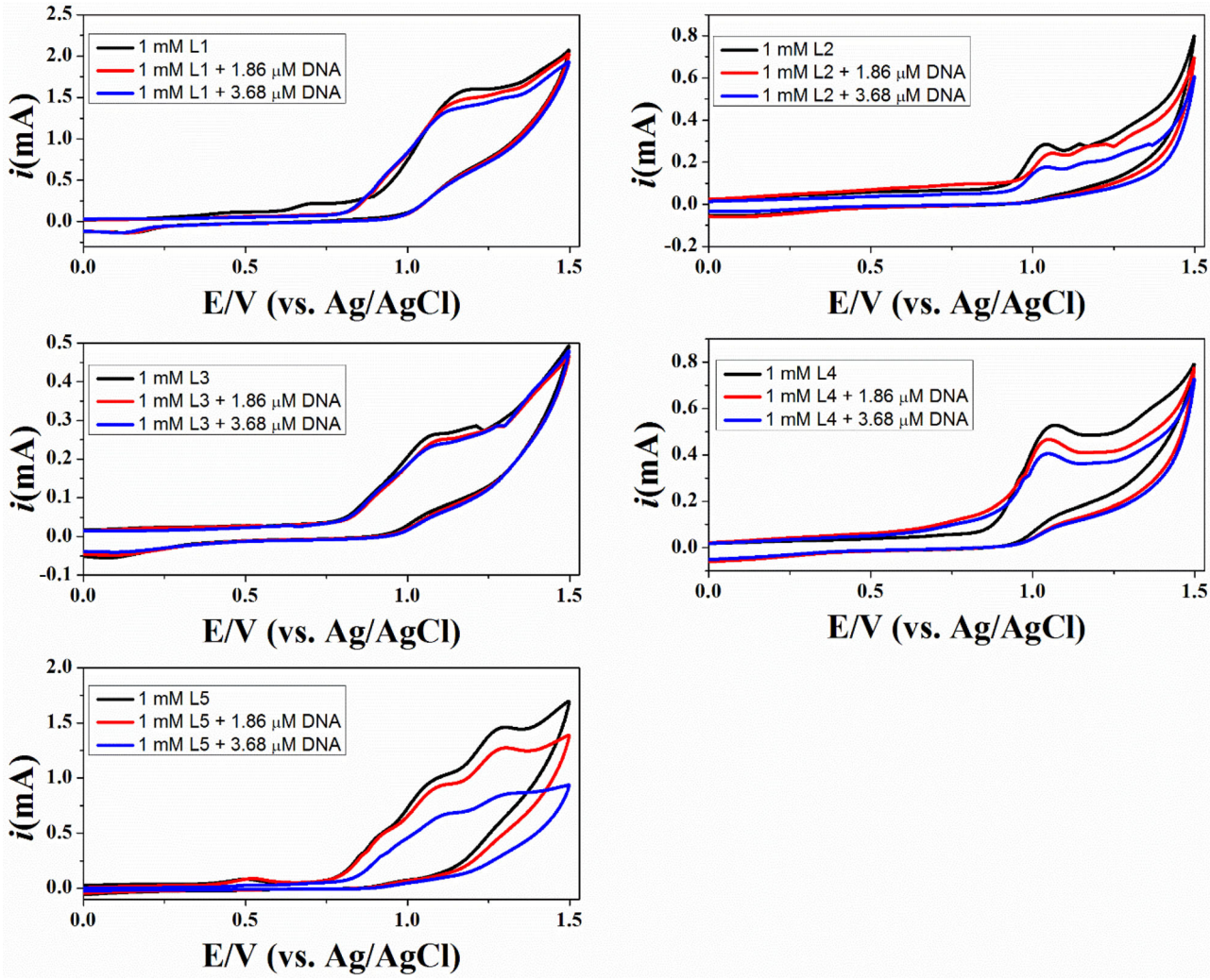

Figure 9. Cyclic voltammograms of 1 mM DMSO solutions of L1, L2, L3, L4 and L5 (—) without DNA, (—) in the presence of 1.86 μM DNA, (—) 3.68 μM DNA on glassy carbon electrode at a scan rate of 100 mV/s.

formed through intercalation. However, binding at the major groove of DNA is also observed for DAPI. An intercalative binding is observed when DAPI binds to RNA (Kapuscinski, 1995; Tanious, Veal, Buczak, Ratmeyer, & Wilson, 1992; Trotta et al., 2003). As reported, DAPI is permeable to dead cells while having a slight permeability in live cells (Gomes et al., 2013). Cell shrinkage and nuclear condensation are salient features of apoptotic cells that can be visualized by DAPI staining and a difference can be assessed as cells undergoing apoptosis possess a slightly smaller nucleus as compared to normal cells (Doonan & Cotter, 2008). The HeLa cells were treated with L5 in 2 different concentrations, i.e. IC_{50} values and 2× IC_{50} values. The images were apprehended after 24 h, demonstrating the cell death mechanism. 4′,6-diamidino-2-phenylindole (DAPI) and its counter stain propidium iodide (PI) were used for staining the nuclear material (Figure 12).

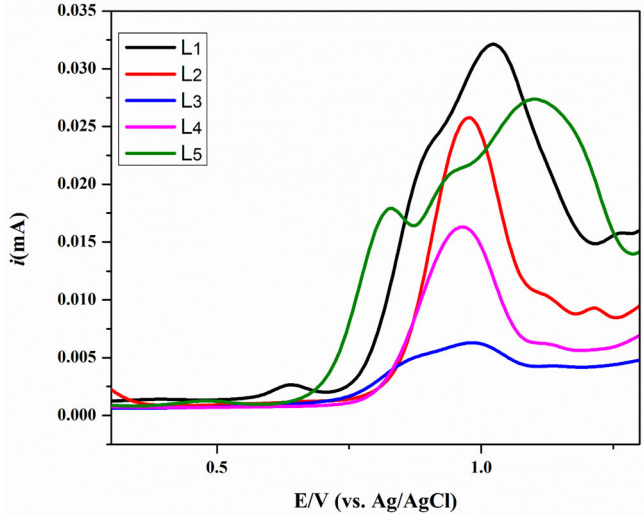

Figure 10. Differential pulse voltammograms of the Schiff base compounds L1 (—), L2 (—), L3 (—), L4 (—), and L5 (—) in 1 mM (15 mL) DMSO solutions, each recorded under argon in the presence of 0.1 M TBAP at 25 °C.

3.8.4. Analysis of intracellular reactive oxygen species (ROS) production

2′,7′-Dichlorodihydrofluorescein diacetate (DCFH-DA) is a fluorescent and cell permeable dye that is intracellularly hydrolyzed to polar form 2′,7′-dichlorodihydrofluroescein (DCFH) by cellular esterase and preserved within the cell

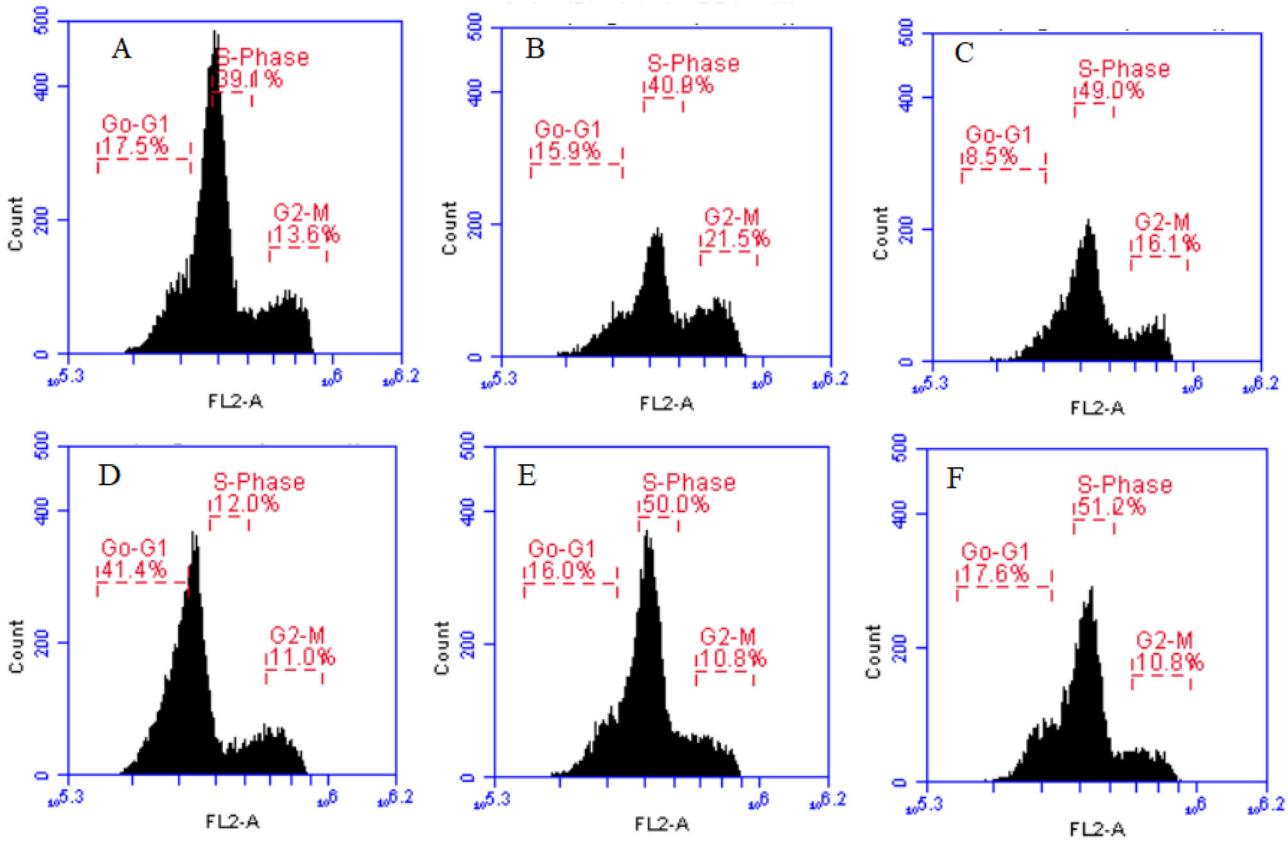

Figure 11. Cell cycle analysis using propidium iodide staining and flow cytometry. Results showing cell population in G0/G1, S and G2/M phases of the cell against HeLa cells at 20 μM (a), 50 μM (b), and 100 μM (c) of L5, negative control (d), 5 μM (e) and 10 μM (f) of carboplatin.

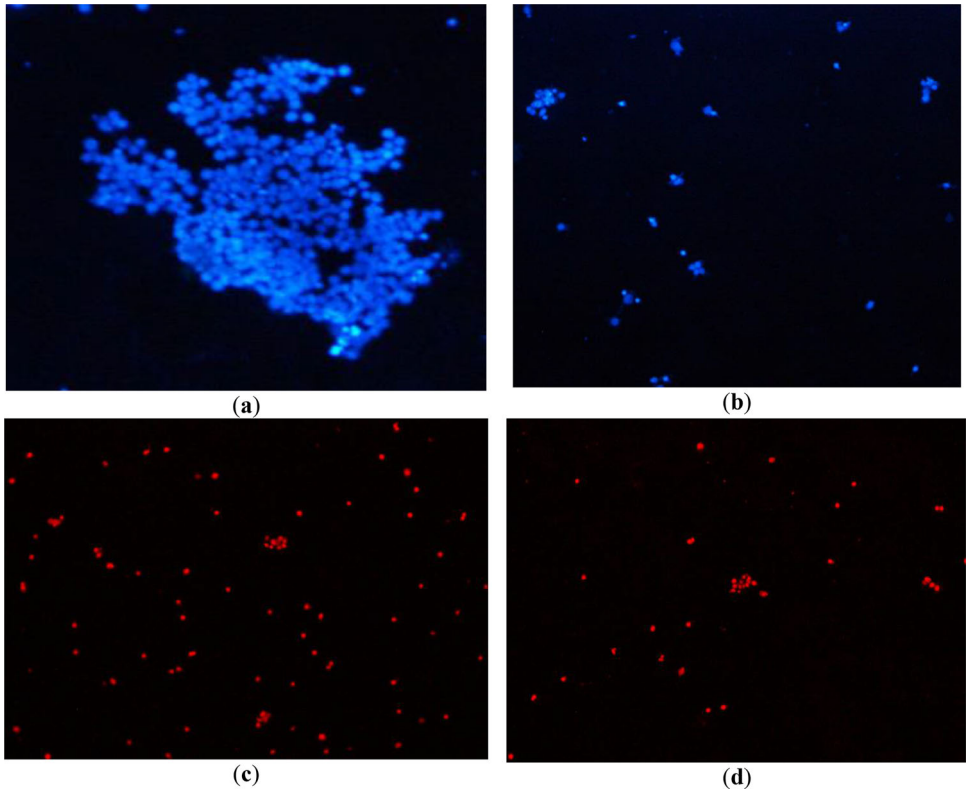

Figure 12. Changes in nuclear morphology induced by IC_{50} 21 μM of L5 (a), 2× IC_{50} 42 μM of L5 (b), after treatment with DAPI. Changes in nuclear morphology induced by IC_{50} 21 μM of L5 (c), 2× IC_{50} 42 μM of L5 (d) after treatment with PI. The changes in nuclear morphology were investigated under a fluorescence microscope (Nikon ECLIPSE Ni–U with the magnification of 10X) against a cervical cancer cell line (HeLa).

(Rastogi et al., 2010). The HeLa cells were treated with the most potent compound L5 in different concentrations (IC_{50} value, i.e. 21 μM and 2× IC_{50}, i.e. 42 μM) and the cells were visualized by fluorescence microscope (Nikon ECLIPSE Ni–U with the magnification of 20×) using an excitation wavelength of 488 nm and emission was detected in the range of 500–600 nm. Figure 13 shows that treated HeLa cells with the potent compound L5 exhibit disintegrated cell membranes and condensed cellular protein (DNA) that may be due to oxidation of lipids and proteins.

3.8.5. Apoptosis assessment by caspase-9 and -3 activity

In three pathways of apoptosis, the role of caspases is crucial for apoptosis induction. Initiator caspases (e.g. caspases-8 and -9) cause activation of executioner caspases (e.g. caspases-3, -6 and -7), which play their role in triggering apoptosis (Elmore, 2007; Szczepaniak et al., 2018). A slight decrease in HeLa cells was found in caspase-9 activity by both the concentrations of compound, i.e. at IC_{50} value (21 μM) and at 2× IC_{50} value (42 μM), as compared to control after an 18 h treatment. However, about 1.8-fold increase in

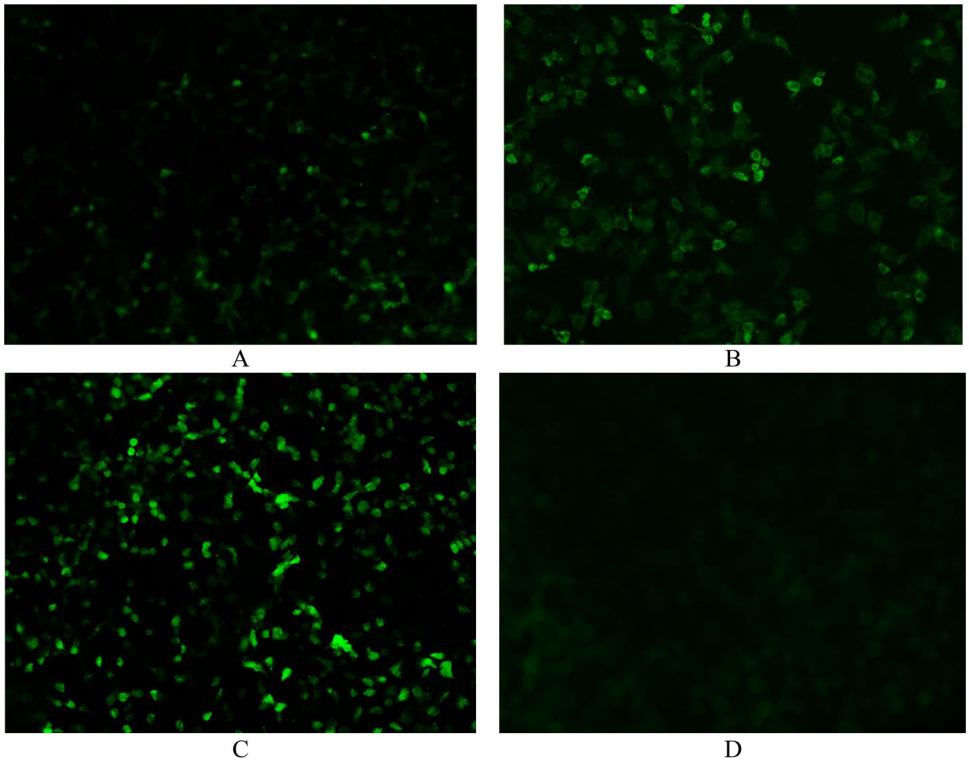

Figure 13. Oxidized DCF fluorescence in HeLa cells induced by IC_{50} 21 μM of L5 (A), 2× IC_{50} 42 μM of L5 (B), carboplatin (C) and untreated cells (D), after treatment with 2′,7′-dichlorodihydrofluorescein diacetate. The images were taken under a fluorescence microscope (Nikon ECLIPSE Ni–U with the magnification of 20×) against a cervical cancer cell line (HeLa).

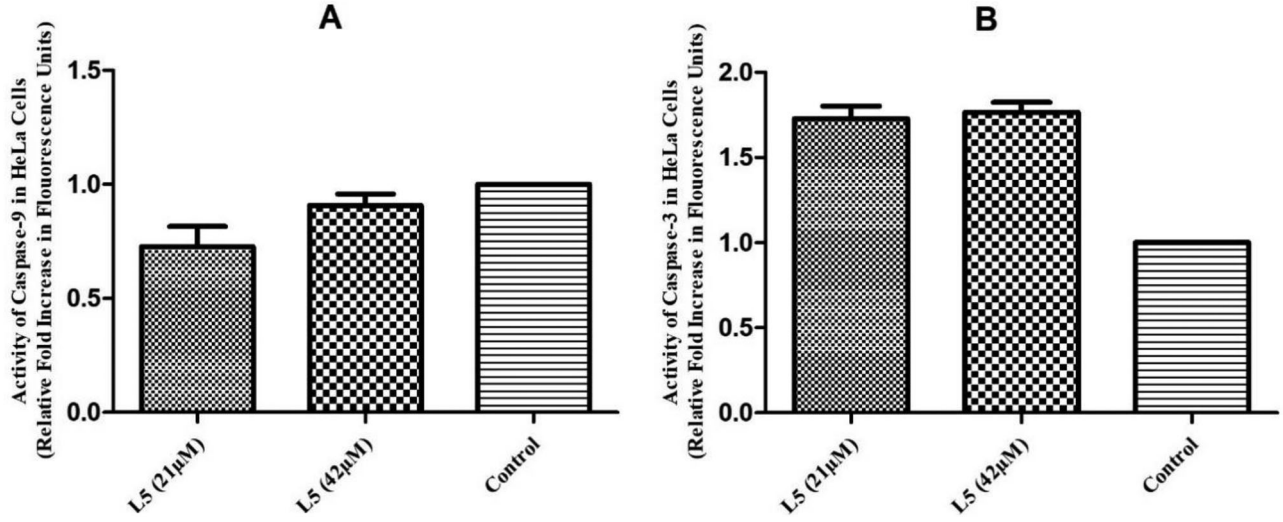

Figure 14. Enhancement of caspase-9 activities after treatment with compound L5 for 18 h (A). Compound L5 stimulates caspase-3 activity and causes apoptosis in HeLa cells (B).

caspase-3 was observed in HeLa cells as compared to control after an 18 h treatment (Figure 14).

4. Conclusion

Five Schiff base compounds (L1–L5) were synthesized and characterized by FT-IR, ^{1}H and ^{13}C NMR spectroscopy, and X-ray crystallography. DNA interaction studies were analyzed by UV–vis spectroscopy and cyclic voltammetry. The binding constants obtained for all compounds from both UV–vis spectroscopy and cyclic voltammetry are in the order of 10^{3}–10^{4} M^{-1} and indicate an electrostatic mode of interaction with DNA. The synthesized azomethines were explored for their antineoplastic effect on HeLa and MCF-7 cancer cell lines, while their cytotoxicity to normal cells was evaluated on a BHK-21 cell line by using the MTT viability assay. The pro-apoptotic mechanism for an active compound was examined by fluorescence microscopy, cell cycle analysis, caspase-9 and -3 activity, reactive oxygen species (ROS) production, and DNA binding studies. Therefore, we suggest that the potent compound L5 could be significant for drug discovery and development in the future having anticancer effects.

Funding

Noor Uddin is thankful to HEC for providing financial support through IRSIP program. Paula L. Diaconescu acknowledges support from NSF Grant CHE-1809116. Saqib Ali is thankful to Quaid-i-Azam University, Islamabad for financial support in the form of URF-2019. Jamshed Iqbal is thankful to the Higher Education Commission of Pakistan for the financial support through Project No.Ph-V-MG-3/Peridot/R&D/HEC/2019 and 6927/NRPU/R&D/17.

Disclosure statement

No potential conflict of interest was reported by the authors.

References

Alaghaz, A., & Bayoumi, H. A. (2013). Synthesis, spectral properties and potentiometric studies on some metal Schiff base complexes derived from 4-chlorophenyl-2-aminothiazole. *International Journal of Electrochemical Science*, *8*, 11860–11876.

Alyar, S., Şen, T., Şen, C., Alyar, H., Adem, Ş., & Özdemir, Ü. Ö. (2019). Synthesis, spectroscopic characterizations, enzyme inhibition, molecular docking study and DFT calculations of new Schiff bases of sulfa drugs. *Journal of Molecular Structure*, *1185*, 416. doi:10.1016/j.molstruc.2019.03.002

Amiri, M., Ajloo, D., Fazli, M., Mokhtarieh, A., Grivani, G., & Saboury, A. A. (2018). Spectroscopic, electrochemical, docking and molecular dynamics studies on the interaction of three oxovanadium (IV) Schiff base complexes with bovine serum albumin and their cytotoxicity against cancer. *Journal of Biomolecular Structure and Dynamics*, *36*(14), 3753–3772. doi:10.1080/07391102.2017.1400467

Armarego, W. L. (2017). Purification of laboratory chemicals. USA: Elsevier, Butterworth-Heinemann.

Arshad, N., & Farooqi, S. I. (2018). Cyclic voltammetric DNA Binding investigations on some anticancer potential metal complexes: A review. *Applied Biochemistry and Biotechnology*, *186*(4), 1090–1110. doi:10.1007/s12010-018-2818-z

Aslanoglu, M., & Ayne, G. (2004). Voltammetric studies of the interaction of quinacrine with DNA. *Analytical and Bioanalytical Chemistry*, *380*(4), 658–663. doi:10.1007/s00216-004-2797-5

Cree, I. A., & Charlton, P. (2017). Molecular chess? Hallmarks of anti-cancer drug resistance. *BMC Cancer*, *17*(1), 10doi:10.1186/s12885-016-2999-1

Crissman, H. A., & Tobey, R. A. (1974). Cell-cycle analysis in 20 minutes. *Science (New York, N.Y.)*, *184*(4143), 1297–1298. doi:10.1126/science.184.4143.1297

Crowley, L. C., Scott, A. P., Marfell, B. J., Boughaba, J. A., Chojnowski, G., & Waterhouse, N. J. (2016). Measuring cell death by propidium iodide uptake and flow cytometry. *Cold Spring Harbor Protocols*, *2016*(7), pdb-prot087163. doi:10.1101/pdb.prot087163

Darzynkiewicz, Z., Halicka, H. D., & Zhao, H. (2010). Analysis of cellular DNA content by flow and laser scanning cytometry. In R. Y. C. Poon (Ed.), *Polyploidization and cancer* (pp. 137–147). New York, NY: Springer.

Dehkhodaei, M., Sahihi, M., & Amiri Rudbari, H. (2018). Spectroscopic and molecular docking studies on the interaction of Pd (II) & Co (II) Schiff base complexes with β-lactoglobulin as a carrier protein. *Journal of Biomolecular Structure and Dynamics*, *36*(12), 3130–3136. doi:10.1080/07391102.2017.1380537

Dengler, W. A., Schulte, J., Berger, D. P., Mertelsmann, R., & Fiebig, H. H. (1995). Development of a propidium iodide fluorescence assay for proliferation and cytotoxicity assays. *Anti-Cancer Drugs*, *6*(4), 522–532. doi:10.1097/00001813-199508000-00005

Deshmukh, P., Soni, P. K., Kankoriya, A., Halve, A. K., & Dixit, R. (2015). 4-Aminoantipyrine: A significant tool for the synthesis of biologically active Schiff bases and metal complexes. *International Journal of Pharmaceutical Sciences and Research*, *34*(1), 162–170.

Doonan, F., & Cotter, T. G. (2008). Morphological assessment of apoptosis. *Methods (San Diego, Calif.)*, *44*(3), 200–204. doi:10.1016/j.ymeth.2007.11.006

Elmore, S. (2007). Apoptosis: A review of programmed cell death. *Toxicologic Pathology*, *35*(4), 495–516. doi:10.1080/01926230701320337

Frisch, M., Trucks, G., Schlegel, H., Scuseria, G. W., Robb, M., Cheeseman, J., … Fox, D. J. (2009). Gaussian 09, Revision E.01 Gaussian, Inc., Wallingford, CT.

Goel, P., Kumar, D., & Chandra, S. (2014). Schiff's base ligands and their transition metal complexes as antimicrobial agents. *Journal of Chemical, Biological and Physical Sciences*, *4*, 1946–1964.

Gomes, F., Ramos, I., Wendt, C., Girard-Dias, W., De Souza, W., Machado, E., & Miranda, E. (2013). New insights into the in situ microscopic visualization and quantification of inorganic polyphosphate stores by 4′, 6-diamidino-2-phenylindole (DAPI)-staining. *European Journal of Histochemistry*, *57*(4), 34. doi:10.4081/ejh.2013.e34

Gottlieb, H. E., Kotlyar, V., & Nudelman, A. (1997). NMR chemical shifts of common laboratory solvents as trace impurities. *The Journal of Organic Chemistry*, *62*(21), 7512–7515. doi:10.1021/jo971176v

Gurova, K. (2009). New hopes from old drugs: Revisiting DNA-binding small molecules as anticancer agents. *Future Oncology*, *5*(10), 1685–1704. doi:10.2217/fon.09.127

Hassanpour, S. H., & Dehghani, M. (2017). Review of cancer from perspective of molecular. *Journal of Cancer Research and Practice*, *4*(4), 127–129. doi:10.1016/j.jcrpr.2017.07.001

Hyndman, I. J. (2016). Review: the Contribution of both nature and nurture to carcinogenesis and progression in solid tumours. *Cancer Microenvironment: Official Journal of the International Cancer Microenvironment Society*, *9*(1), 63–69. doi:10.1007/s12307-016-0183-4

Hyndman, I. J. (2016). The contribution of both nature and nurture to carcinogenesis and progression in solid tumours. *Cancer Microenvironment*, *9*(1), 63–69. doi:10.1007/s12307-016-0183-4

Iqbal, J., Ejaz, S. A., Saeed, A., & Al-Rashida, M. (2018). Detailed investigation of anticancer activity of sulfamoyl benz (sulfon) amides and 1H-pyrazol-4-yl benzamides: An experimental and computational study. *European Journal of Pharmacology*, *832*, 11–24.

Iqbal, M., Ahmad, I., Ali, S., Muhammad, N., Ahmed, S., & Sohail, M. (2013). Dimeric "paddle-wheel" carboxylates of copper (II): Synthesis,

crystal structure and electrochemical studies. *Polyhedron*, *50*(1), 524–531. doi:10.1016/j.poly.2012.11.037

Jeyaraman, P., Alagarraj, A., & Natarajan, R. (2019). In silico and in vitro studies of transition metal complexes derived from curcumin–isoniazid Schiff base. *Journal of Biomolecular Structure and Dynamics*, *37*, 1–12. doi:10.1080/07391102.2019.1581090

Kajal, A., Bala, S., Kamboj, S., Sharma, N., & Saini, V. (2013). Schiff bases: A versatile pharmacophore. *Journal of Catalysts*, *2013*, 1. doi:10.1155/2013/893512

Kapuscinski, J. (1995). DAPI: A DNA-specific fluorescent probe. *Biotechnic & Histochemistry*, *70*(5), 220–233. doi:10.3109/10520299509108199

Kim, S. (2015). New and emerging factors in tumorigenesis: An overview. *Cancer Management and Research*, *7*, 225doi:10.2147/CMAR.S47797

Kumaran, J. S., Priya, S., Gowsika, J., Jayachandramani, N., & Mahalakshmi, S. (2013). Synthesis, spectroscopic characterization, in silica DNA studies and antibacterial activities of copper (II) and zinc (II) complexes derived from thiazole based pyrazolone derivatives. *Research Journal of Pharmaceutical, Biological and Chemical Science*, *4*(279), e287.

Kutzelnigg, W., Fleischer, U., & Schindler, M. (1990). In Diehl, P., Fluck, and Kosfeld, R. (Eds.), *NMR basic principles and progress*. Springer, Berlin, 23, 165.

Lin, G.-J., Jiang, G.-B., Xie, Y.-Y., Huang, H.-L., Liang, Z.-H., & Liu, Y.-J. (2013). Cytotoxicity, apoptosis, cell cycle arrest, reactive oxygen species, mitochondrial membrane potential, and Western blotting analysis of ruthenium (II) complexes. *JBIC Journal of Biological Inorganic Chemistry*, *18*(8), 873–882. doi:10.1007/s00775-013-1032-2

Lin, S.-F., Lin, J.-D., Hsueh, C., Chou, T.-C., & Wong, R. J. (2018). Activity of roniciclib in medullary thyroid cancer. *Oncotarget*, *9*(46), 28030doi:10.18632/oncotarget.25555

Mosmann, T. (1983). Rapid colorimetric assay for cellular growth and survival: Application to proliferation and cytotoxicity assays. *Journal of Immunological Methods*, *65*(1–2), 55–63. doi:10.1016/0022-1759(83)90303-4

Niks, M. (1990). Towards an optimized MTT assay. *Journal of Immunological Methods*, *130*(1), 149–151. doi:10.1016/0022-1759(90)90309-j

Nunez, R. (2001). DNA measurement and cell cycle analysis by flow cytometry. *Current Issues in Molecular Biology*, *3*(3), 67–70.

Olsson, M., & Zhivotovsky, B. (2011). Caspases and cancer. *Cell Death & Differentiation*, *18*(9), 1441. doi:10.1038/cdd.2011.30

Pan, J., Xu, G., & Yeung, S.-C. J. (2001). Cytochrome c release is upstream to activation of caspase-9, caspase-8, and caspase-3 in the enhanced apoptosis of anaplastic thyroid cancer cells induced by manumycin and paclitaxel. *Journal of Clinical Endocrinology & Metabolism*, *86*(10), 4731–4740. doi:10.1210/jc.86.10.4731

Popovic, Z., Roje, Z., & Pavlovic, G. (2001). Matkovic-Calogovic D and Giester G. *Journal of Molecular Structure*, *2001*, 597.

Rambabu, A., Pradeep Kumar, M., Ganji, N., Daravath, S. & Shivaraj, (2019). DNA binding and cleavage, cytotoxicity and antimicrobial studies of Co (II), Ni (II), Cu (II) and Zn (II) complexes of 1-((E)-(4-(trifluoromethoxy) phenylimino) methyl) naphthalen-2-ol Schiff base. *Journal of Biomolecular Structure and Dynamics*, 1–10.

Rastogi, R. P., , Singh, S. P., Hader, D.-P., & Sinha, R. P. (2010). Detection of reactive oxygen species (ROS) by the oxidant sensing probe 2',7'-dichlorodihydrofluorescein diacetate in the cyanobacterium Anabaena variabilis PCC 7937. *Biochemical and Biophysical Research Communications*, *397*(3), 603–607. doi:10.1016/j.bbrc.2010.06.006

Saito, Y., Uchida, N., Tanaka, S., Suzuki, N., Tomizawa-Murasawa, M., Sone, A., … Ishikawa, F. (2010). Induction of cell cycle entry eliminates human leukemia stem cells in a mouse model of AML. *Nature Biotechnology*, *28*(3), 275. doi:10.1038/nbt.1607

Shabbir, M., Akhter, Z., Ahmad, I., Ahmed, S., Bolte, M., & McKee, V. (2017). Synthesis and bioelectrochemical behavior of aromatic amines. *Bioorganic Chemistry*, *75*, 224–234.

Shabbir, M., Akhter, Z., Ahmad, I., Ahmed, S., Ismail, H., Mirza, B., … Bolte, M. (2015). Synthesis, biological and electrochemical evaluation of novel nitroaromatics as potential anticancerous drugs. *Bioelectrochemistry*, *104*, 85–92. doi:10.1016/j.bioelechem.2015.03.007

Shahraki, S., & Heydari, A. (2018). Binding forces between a novel Schiff base palladium (II) complex and two carrier proteins: Human serum albumi and β-lactoglobulin. *Journal of Biomolecular Structure and Dynamics*, *36*(11), 2807–2821. doi:10.1080/07391102.2017.1367723

Shahraki, S., Shiri, F., & Saeidifar, M. (2018). Synthesis, characterization, in silico ADMET prediction, and protein binding analysis of a novel zinc (II) Schiff-base complex: Application of multi-spectroscopic and computational techniques. *Journal of Biomolecular Structure and Dynamics*, *36*(7), 1666–1680. doi:10.1080/07391102.2017.1334595

Shokohi-Pour, Z., Chiniforoshan, H., Sabzalian, M. R., Esmaeili, S.-A., & Momtazi-Borojeni, A. A. (2018). Cobalt (II) complex with novel unsymmetrical tetradentate Schiff base (ON) ligand: In vitro cytotoxicity studies of complex, interaction with DNA/protein, molecular docking studies, and antibacterial activity. *Journal of Biomolecular Structure and Dynamics*, *36*(2), 532–549. doi:10.1080/07391102.2017.1287006

Siddiqui, H., Iqbal, A., Ahmad, S., & Weaver, W. (2006). Synthesis and spectroscopic studies of new Schiff bases. *Molecules (Basel, Switzerland)*, *11*(2), 206–211. doi:10.3390/11020206

Sirajuddin, M., Ali, S., & Badshah, A. (2013). Drug–DNA interactions and their study by UV–Visible, fluorescence spectroscopies and cyclic voltametry. *Journal of Photochemistry and Photobiology B: Biology*, *124*, 1–19. doi:10.1016/j.jphotobiol.2013.03.013

Sirajuddin, M., Ali, S., McKee, V., Zaib, S., & Iqbal, J. (2014). Organotin (IV) carboxylate derivatives as a new addition to anticancer and antileishmanial agents: Design, physicochemical characterization and interaction with Salmon sperm DNA. *RSC Adv.*, *4*(101), 57505–57521. doi:10.1039/C4RA10487K

Sirajuddin, M., Ali, S., Shah, N. A., Khan, M. R., & Tahir, M. N. (2012). Synthesis, characterization, biological screenings and interaction with calf thymus DNA of a novel azomethine 3-((3, 5-dimethylphenylimino) methyl) benzene-1, 2-diol. *Spectrochimica Acta Part A: Molecular and Biomolecular Spectroscopy*, *94*, 134–142. doi:10.1016/j.saa.2012.03.068

Sträuber, H., & Müller, S. (2010). Viability states of bacteria—Specific mechanisms of selected probes. *Cytometry Part A*, *77*(7), 623–634. doi:10.1002/cyto.a.20920

Szczepaniak, J., Strojny, B., Chwalibog, E. S., Jaworski, S., Jagiello, J., Winkowska, M., … Grodzik, M. (2018). Effects of reduced graphene oxides on apoptosis and cell cycle of glioblastoma multiforme. *International Journal of Molecular Sciences*, *19*(12), 3939. doi:10.3390/ijms19123939

Tanious, F. A., Veal, J. M., Buczak, H., Ratmeyer, L. S., & Wilson, W. D. (1992). DAPI (4′, 6-diamidino-2-phenylindole) binds differently to DNA and RNA: Minor-groove binding at AT sites and intercalation at AU sites. *Biochemistry*, *31*(12), 3103–3112. doi:10.1021/bi00127a010

Trotta, E., Del Grosso, N., Erba, M., Melino, S., Cicero, D., & Paci, M. (2003). Interaction of DAPI with individual strands of trinucleotide repeats: Effects on replication in vitro of the AAT·ATT triplet. *European Journal of Biochemistry*, *270*(23), 4755–4761. doi:10.1046/j.1432-1033.2003.03877.x

Uddin, M. N., Siddique, Z. A., Mase, N., Uzzaman, M., & Shumi, W. (2019). Oxotitanium (IV) complexes of some bis-unsymmetric Schiff bases: Synthesis, structural elucidation and biomedical applications. *Applied Organometallic Chemistry*, *33*(6), e4876. doi:10.1002/aoc.4876

Virnig, B. A., Baxter, N. N., Habermann, E. B., Feldman, R. D., & Bradley, C. J. (2009). A matter of race: Early-versus late-stage cancer diagnosis. *Health Affairs*, *28*(1), 160–168. doi:10.1377/hlthaff.28.1.160

Zehra, S., Shavez Khan, M., Ahmad, I., & Arjmand, F. (2019). New tailored substituted benzothiazole Schiff base Cu (II)/Zn (II) antitumor drug entities: Effect of substituents on DNA binding profile, antimicrobial and cytotoxic activity. *Journal of Biomolecular Structure and Dynamics*, *37*(7), 1863–1879. doi:10.1080/07391102.2018.1467794

Zhang, Z., Bi, C., Fan, Y., Wang, H., & Bao, Y. (2015). Cefepime, a fourth-generation cephalosporin, in complex with manganese, inhibits proteasome activity and induces the apoptosis of human breast cancer cells. *International Journal of Molecular Medicine*, *36*(4), 1143–1150. doi:10.3892/ijmm.2015.2297